

Holographic Schwinger effect in a soft wall AdS/QCD model

Yue Ding¹ and Zi-qiang Zhang^{1,*}

¹*School of Mathematics and Physics, China University of Geosciences, Wuhan 430074, China*

We perform the potential analysis for the holographic Schwinger effect in a deformed AdS_5 model with conformal invariance broken by a background dilaton. We evaluate the static potential by analyzing the classical action of a string attaching the rectangular Wilson loop on a probe D3 brane sitting at an intermediate position in the bulk AdS space. We observe that the inclusion of chemical potential tends to enhance the production rate, reverse to the effect of confining scale. Also, we calculate the critical electric field by Dirac-Born-Infeld (DBI) action.

PACS numbers: 11.25.Tq, 11.15.Tk, 11.25-w

I. INTRODUCTION

Schwinger effect is an interesting phenomenon in quantum electrodynamics (QED): virtual electron-positron pairs can be materialized and become real particles due to the presence of a strong electric field. The production rate Γ (per unit time and unit volume) was first calculated by Schwinger for weak-coupling and weak-field in 1951 [1]

$$\Gamma \sim \exp\left(\frac{-\pi m^2}{eE}\right), \quad (1)$$

where E , m and e are the external electric field, electron mass and elementary electric charge, respectively. In this case, there is no critical field trivially. Thirty-one years later, Affleck et.al generalized it to the case for arbitrary-coupling and weak-field [2]

$$\Gamma \sim \exp\left(\frac{-\pi m^2}{eE} + \frac{e^2}{4}\right), \quad (2)$$

in this case, the exponential suppression vanishes when E reaches $E_c = (4\pi/e^3)m^2 \simeq 137m^2/e$. Obviously, the critical field E_c does not satisfy the weak-field condition, i.e., $eE \ll m^2$. Thus, it seems that one could not find out E_c under the weak-field condition. One step further, one doesn't know whether the catastrophic decay really occurs or not.

Actually, the Schwinger effect is not unique to QED, but a universal aspect of quantum field theories (QFTs) coupled to an U(1) gauge field. However, it remains difficult to study this effect in a QCD-like or confining theory using QFTs since the (original) Schwinger effect must be non-perturbative. Fortunately, the AdS/CFT correspondence [3–5] may provide an alternative way. In 2011, Semenoff and Zarembo proposed [6] a holographic set-up to study the Schwinger effect in the higgsed $\mathcal{N} = 4$ supersymmetric Yang-Mills theory (SYM). They found that at large N and large 't Hooft coupling λ

$$\Gamma \sim \exp\left[-\frac{\sqrt{\lambda}}{2}\left(\sqrt{\frac{E_c}{E}} - \sqrt{\frac{E}{E_c}}\right)^2\right], \quad E_c = \frac{2\pi m^2}{\sqrt{\lambda}}, \quad (3)$$

interestingly, the value of E_c coincides with the one obtained from the DBI action [7]. Subsequently, Sato and Yoshida argued that [8] the Schwinger effect can be studied by potential analysis. Specifically, the pair production can be estimated by a static potential, consisting of static mass energies, an electric potential from an external electric-field, and the Coulomb potential between a particle-antiparticle pair. The shapes of the potential depend on the external field E (see fig.1). When $E < E_c$, the potential barrier is present and the Schwinger effect could occur as a tunneling process. As E increases, the barrier decreases and gradually disappears at $E = E_c$. When $E > E_c$, the vacuum becomes catastrophically unstable. Further studies of the Schwinger effect in this direction can be found, e.g., in [9–19]. On the other hand, the holographic Schwinger effect has been investigated from the imaginary part of a probe brane action [20–23]. For a recent review on this topic, see [24].

Here we present an alternative holographic approach to study the Schwinger effect using potential analysis. The motivation is that holographic QCD models, like hard wall [25, 26], soft wall [27] and some improved AdS/QCD

*Electronic address: zhangzq@cug.edu.cn

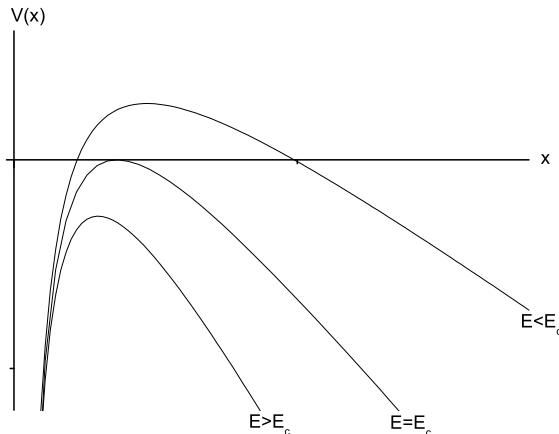


FIG. 1: $V(x)$ versus x with $V(x) = 2m - eEx - \frac{\alpha_s}{x}$, where α_s denotes the fine-structure constant.

models [28–34] have achieved considerable success in describing various aspects of hadron physics. In particular, we will adopt the $SW_{T,\mu}$ model [35] which is defined by the AdS with a charged black hole to describe finite temperature and density multiplied by a warp factor to generate confinement. It turns out that such a model can provide a good phenomenological description of quark-antiquark interaction. Also, the resulting deconfinement line in $\mu - T$ plane is similar to that obtained by lattice and effective models of QCD (for further studies of models of this type, see [36–41]). Motivated by this, in this paper we study the Schwinger effect in the $SW_{T,\mu}$ model. Specifically, we want to understand how the Schwinger effect is affected by chemical potential and confining scale. Also, this work could be considered as an extension of [8] to the case with chemical potential and confining scale.

The outline of the paper is as follows. In the next section, we briefly review the $SW_{T,\mu}$ model given in [35]. In section 3, we perform the potential analysis for the Schwinger effect in the $SW_{T,\mu}$ model and investigate how chemical potential and confining scale affect the production rate. Also, we calculate the critical field from DBI action. Finally, we conclude our results in section 4.

II. SETUP

This section is devoted to a short introduction of the $SW_{T,\mu}$ model proposed in [35]. The metric of the model in the string frame takes the form

$$ds^2 = \frac{R^2}{z^2} h(z) (-f(z) dt^2 + d\vec{x}^2 + \frac{dz^2}{f(z)}), \quad (4)$$

with

$$f(z) = 1 - (1 + Q^2) \left(\frac{z}{z_h}\right)^4 + Q^2 \left(\frac{z}{z_h}\right)^6, \quad h(z) = e^{c^2 z^2}, \quad (5)$$

where R is the AdS radius. Q represents the charge of black hole. z denotes the fifth coordinate with $z = z_h$ the horizon, defined by $f(z_h) = 0$. The warp factor $h(z)$, characterizing the soft wall model, distorts the metric and brings the confining scale c (see [28] for an analytical way to introduce the warp factor by potential reconstruction approach).

The temperature of the black hole is

$$T = \frac{1}{\pi z_h} \left(1 - \frac{Q^2}{2}\right), \quad 0 \leq Q \leq \sqrt{2}. \quad (6)$$

The chemical potential is

$$\mu = \sqrt{3}Q/z_h. \quad (7)$$

Note that for $Q = 0$, the $SW_{T,\mu}$ model reduces to the Andreev model [42]. For $c = 0$, it becomes the AdS-Reissner Nordstrom black hole [43, 44]. For $Q = c = 0$, it returns to AdS black hole.

III. POTENTIAL ANALYSIS IN (HOLOGRAPHIC) SCHWINGER EFFECT

In this section, we follow the argument in [8] to study the behavior of the Schwinger effect in the $SW_{T,\mu}$ model. Since the calculations of [8] were performed using the radial coordinate $r = R^2/z$. For contrast, we use coordinate r as well.

The Nambu-Goto action is

$$S = T_F \int d\tau d\sigma \mathcal{L} = T_F \int d\tau d\sigma \sqrt{g}, \quad T_F = \frac{1}{2\pi\alpha'}, \quad (8)$$

where α' is related to λ by $\frac{R^2}{\alpha'} = \sqrt{\lambda}$. g represents the determinant of the induced metric

$$g_{\alpha\beta} = g_{\mu\nu} \frac{\partial X^\mu}{\partial \sigma^\alpha} \frac{\partial X^\nu}{\partial \sigma^\beta}, \quad (9)$$

with $g_{\mu\nu}$ the metric and X^μ the target space coordinate.

Supposing the pair axis is aligned in one direction, e.g., x_1 direction,

$$t = \tau, \quad x_1 = \sigma, \quad x_2 = 0, \quad x_3 = 0, \quad r = r(\sigma). \quad (10)$$

Under this ansatz, the induced metric reads

$$g_{00} = \frac{r^2 h(r) f(r)}{R^2}, \quad g_{01} = g_{10} = 0, \quad g_{11} = \frac{r^2 h(r)}{R^2} + \frac{R^2 h(r)}{r^2 f(r)} \left(\frac{dr}{d\sigma}\right)^2, \quad (11)$$

then the Lagrangian density becomes

$$\mathcal{L} = \sqrt{M(r) + N(r) \left(\frac{dr}{d\sigma}\right)^2}, \quad (12)$$

with

$$M(r) = \frac{r^4 h^2(r) f(r)}{R^4}, \quad N(r) = h^2(r). \quad (13)$$

As \mathcal{L} does not depend on σ explicitly, the Hamiltonian is conserved,

$$\mathcal{L} - \frac{\partial \mathcal{L}}{\partial \left(\frac{dr}{d\sigma}\right)} \left(\frac{dr}{d\sigma}\right) = \text{Constant}. \quad (14)$$

Imposing the boundary condition at the tip of the minimal surface,

$$\frac{dr}{d\sigma} = 0, \quad r = r_c \quad (r_t < r_c < r_0), \quad (15)$$

one gets

$$\frac{dr}{d\sigma} = \sqrt{\frac{M^2(r) - M(r)M(r_c)}{M(r_c)N(r)}}, \quad (16)$$

with $M(r_c) = M(r)|_{r=r_c}$. Here $r = r_t$ is the horizon. $r = r_0$ is an intermediate position, which can yield a finite mass [6]. The configuration of the string world-sheet is depicted in fig.2.

Integrating (16) with the boundary condition (15), the inter-distance of the particle pair is obtained

$$x = 2 \int_{r_c}^{r_0} \frac{d\sigma}{dr} dr = 2 \int_{r_c}^{r_0} dr \sqrt{\frac{M(r_c)N(r)}{M^2(r) - M(r)M(r_c)}}. \quad (17)$$

On the other hand, plugging (12) into (8), the sum of Coulomb potential and static energy is given by

$$V_{CP+E} = 2T_F \int_{r_c}^{r_0} dr \sqrt{\frac{M(r)N(r)}{M(r) - M(r_c)}}. \quad (18)$$

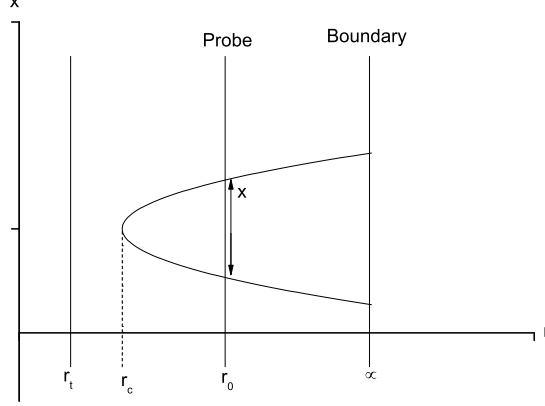


FIG. 2: The configuration of the string world-sheet.

The next task is to calculate the critical field. The DBI action is

$$S_{DBI} = -T_{D3} \int d^4x \sqrt{-\det(G_{\mu\nu} + \mathcal{F}_{\mu\nu})}, \quad (19)$$

with

$$T_{D3} = \frac{1}{g_s(2\pi)^3\alpha'^2}, \quad \mathcal{F}_{\mu\nu} = 2\pi\alpha' F_{\mu\nu}, \quad (20)$$

where T_{D3} is the D3-brane tension.

The induced metric is

$$G_{00} = -\frac{r^2 h(r) f(r)}{R^2}, \quad G_{11} = G_{22} = G_{33} = \frac{r^2 h(r)}{R^2}. \quad (21)$$

Supposing the electric field is turned on along x_1 direction [8], then

$$G_{\mu\nu} + \mathcal{F}_{\mu\nu} = \begin{pmatrix} -\frac{r^2 h(r) f(r)}{R^2} & 2\pi\alpha' E & 0 & 0 \\ -2\pi\alpha' E & \frac{r^2 h(r)}{R^2} & 0 & 0 \\ 0 & 0 & \frac{r^2 h(r)}{R^2} & 0 \\ 0 & 0 & 0 & \frac{r^2 h(r)}{R^2} \end{pmatrix}, \quad (22)$$

results in

$$\det(G_{\mu\nu} + \mathcal{F}_{\mu\nu}) = \frac{r^4 h^2(r)}{R^4} [(2\pi\alpha')^2 E^2 - \frac{r^4 h^2(r) f(r)}{R^4}]. \quad (23)$$

Substituting (23) into (19) and making the probe D3-brane located at $r = r_0$, one finds

$$S_{DBI} = -T_{D3} \frac{r_0^2 h(r_0)}{R^2} \int d^4x \sqrt{\frac{r_0^4 h^2(r_0) f(r_0)}{R^4} - (2\pi\alpha')^2 E^2}, \quad (24)$$

with $f(r_0) = f(r)|_{r=r_0}$, $h(r_0) = h(r)|_{r=r_0}$.

To avoid (24) being ill-defined, one gets

$$\frac{r_0^4 h^2(r_0) f(r_0)}{R^4} - (2\pi\alpha')^2 E^2 \geq 0, \quad (25)$$

yielding

$$E \leq T_F \frac{r_0^2 h(r_0)}{R^2} \sqrt{f(r_0)}. \quad (26)$$

As a result, the critical field is

$$E_c = T_F \frac{r_0^2 h(r_0)}{R^2} \sqrt{f(r_0)}, \quad (27)$$

one can see that E_c depends on T , μ and c .

Next, we calculate the total potential. For the sake of notation simplicity, we introduce the following dimensionless parameters

$$\alpha \equiv \frac{E}{E_c}, \quad y \equiv \frac{r}{r_c}, \quad a \equiv \frac{r_c}{r_0}, \quad b \equiv \frac{r_t}{r_0}. \quad (28)$$

Given that, the total potential reads

$$\begin{aligned} V_{tot}(x) &= V_{CP+E} - Ex \\ &= 2ar_0 T_F \int_1^{1/a} dy \sqrt{\frac{A(y)B(y)}{A(y) - A(y_c)}} \\ &\quad - 2ar_0 T_F \alpha \frac{r_0^2 h(y_0)}{R^2} \sqrt{f(y_0)} \int_1^{1/a} dy \sqrt{\frac{A(y_c)B(y)}{A^2(y) - A(y)A(y_c)}}, \end{aligned} \quad (29)$$

with

$$\begin{aligned} A(y) &= \frac{(ar_0 y)^4 h^2(y) f(y)}{R^4}, & A(y_c) &= \frac{(ar_0)^4 h^2(y_c) f(y_c)}{R^4}, & B(y) &= h^2(y), \\ h(y) &= e^{\frac{c^2 R^4}{(ar_0 y)^2}}, & f(y) &= 1 - \left(1 + \frac{\mu^2 R^4}{3r_t^2}\right) \left(\frac{b}{ay}\right)^4 + \frac{\mu^2 R^4}{3r_t^2} \left(\frac{b}{ay}\right)^6, \\ h(y_c) &= e^{\frac{c^2 R^4}{(ar_0)^2}}, & f(y_c) &= 1 - \left(1 + \frac{\mu^2 R^4}{3r_t^2}\right) \left(\frac{b}{a}\right)^4 + \frac{\mu^2 R^4}{3r_t^2} \left(\frac{b}{a}\right)^6, \\ h(y_0) &= e^{\frac{c^2 R^4}{r_0^2}}, & f(y_0) &= 1 - \left(1 + \frac{\mu^2 R^4}{3r_t^2}\right) b^4 + \frac{\mu^2 R^4}{3r_t^2} b^6, \end{aligned} \quad (30)$$

we have checked that by taking $c = \mu = 0$ in (29), the result of $\mathcal{N} = 4$ SYM [8] is regained.

Before going further, we discuss the value of c . In this work we tend to study the behavior of the holographic Schwinger effect in a class of models parametrized by c . To that end, we make c dimensionless by normalizing it at fixed temperatures and express other quantities, e.g. μ , in units of it. In [45], the authors found that the range of $0 \leq c/T \leq 2.5$ is most relevant for a comparison with QCD. We use that range.

In fig.3, we plot $V_{tot}(x)$ as a function of x for $\mu/T = 1$ and $c/T = 0.1$ (other cases with different values of μ/T and c/T have similar picture), where we have set $b = 0.5$ and $T_F r_0 = R^2/r_0 = 1$, as follows from [8]. From these figures, one can see that there exists a critical electric field at $\alpha = 1$ ($E = E_c$), and for $\alpha < 1$ ($E < E_c$), the potential barrier is present, in agreement with [8].

To see how chemical potential modifies the Schwinger effect, we plot $V_{tot}(x)$ versus x with fixed c/T for different values of μ/T in fig.4. The left panel is for $c/T = 0.1$ and the right $c/T = 2.5$. In both panels from top to bottom $\mu/T = 0, 1, 5$, respectively. One can see that at fixed c/T , as μ/T increases, the height and width of the potential barrier both decrease. As we know, the higher or the wider the potential barrier, the harder the produced pairs escape to infinity. Thus, one concludes that the inclusion of chemical potential decrease the potential barrier thus enhancing the Schwinger effect, in accordance with the findings of [14].

Also, we plot $V_{tot}(x)$ against x with fixed μ/T for different values of c/T in fig.5. One finds at fixed μ/T , the height and width of the potential barrier both increase as c/T increases, implying the presence of confining scale reduces the Schwinger effect, reverse to the effect of chemical potential.

Finally, to understand how chemical potential and confining scale affect the critical electric field, we plot E_c/E_{c0} versus μ/T (c/T) in the left (right) panel of fig.6, where E_{c0} denotes the critical electric field of SYM. One can see that E_c/E_{c0} decreases as μ/T increases, indicating the chemical potential decreases E_c thus enhancing the Schwinger effect. Meanwhile, the confining scale has an opposite effect, consistently with the potential analysis. Furthermore, it can be seen that E_c/E_{c0} can be larger or smaller than one, which means that the $SW_{T,\mu}$ model may provide a wider range of the Schwinger effect in comparison to SYM.

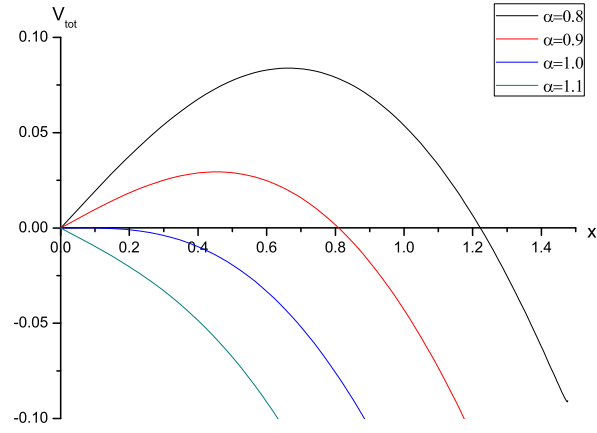


FIG. 3: $V_{tot}(x)$ versus x with $\mu/T = 1$, $c/T = 0.1$. In the plots from top to bottom $\alpha = 0.8, 0.9, 1.0, 1.1$, respectively.

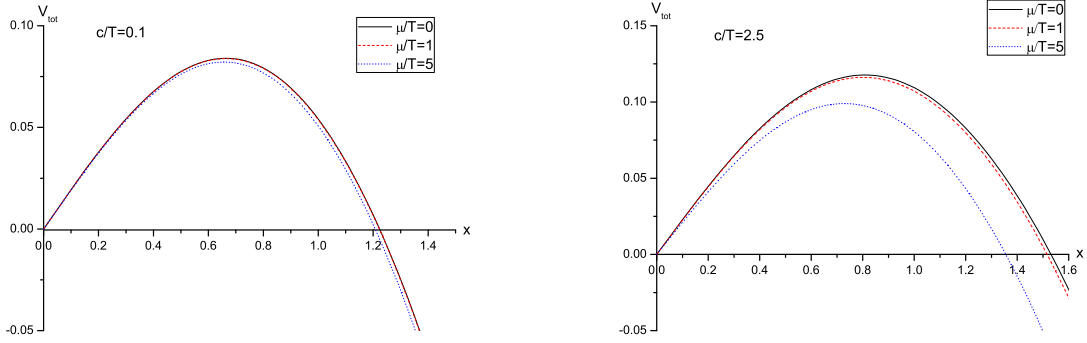


FIG. 4: $V_{tot}(x)$ versus x with $\alpha = 0.8$ and fixed c/T for different values of μ/T . In both plots from top to bottom $\mu/T = 0, 1, 5$, respectively.

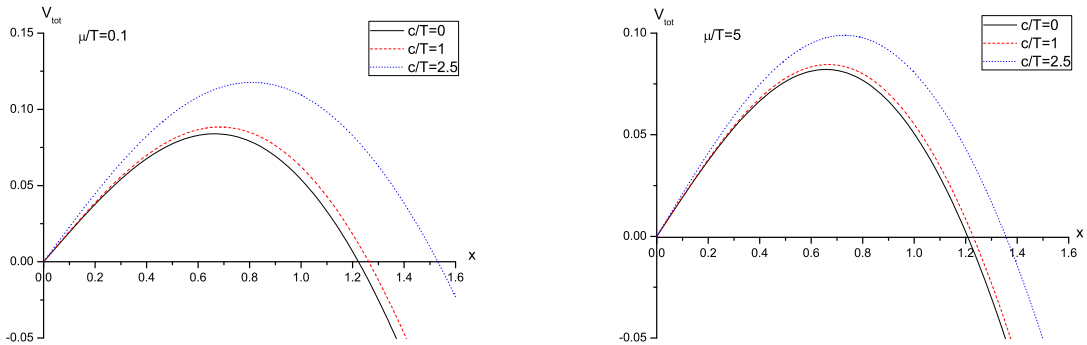


FIG. 5: $V_{tot}(x)$ versus x with $\alpha = 0.8$ and fixed μ/T for different values of c/T . In both plots from top to bottom $c/T = 2.5, 1, 0$, respectively.

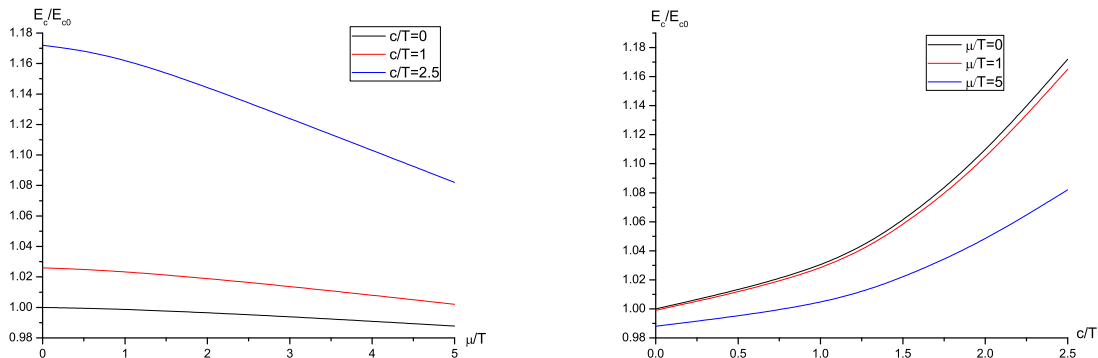


FIG. 6: Left: E_c/E_{c0} versus μ/T , from top to bottom $c/T = 2.5, 1, 0$, respectively. Right: E_c/E_{c0} versus c/T , from top to bottom $\mu/T = 0, 1, 5$, respectively.

IV. CONCLUSION

The study of Schwinger effect in non-conformal plasma under the influence of chemical potential may shed some light on heavy ion collisions. In this paper, we investigated the effect of chemical potential and confining scale on the holographic Schwinger effect in a soft wall AdS/QCD model. We analyzed the electrostatic potentials by evaluating the classical action of a string attaching the rectangular Wilson loop on a probe D3 brane sitting at an intermediate position in the bulk AdS and calculated the critical electric field from DBI action. We found that the inclusion of chemical potential tends to decrease the potential barrier thus enhancing the production rate, reverse to the effect of confining scale. Moreover, we observed with some chosen values of μ/T and c/T , E_c can be larger or smaller than its counterpart of SYM, implying the $SW_{T,\mu}$ model may provide theoretically a wider range of the Schwinger effect in comparison to SYM.

However, there are some questions need to be studied further. First, the potential analysis are basically within the Coulomb branch, related to the leading exponent corresponding to the on-shell action of the instanton, not the full decay rate. Also, the $SW_{T,\mu}$ model is not a consistent model since it does not solve the full set of equations of motion. Performing such analysis in some consistent models, e.g. [28–34] would be instructive (usually the metrics of those models are only known numerically, so the calculations are more challenging).

V. ACKNOWLEDGMENTS

This work is supported by the NSFC under Grant No. 11705166 and the Fundamental Research Funds for the Central Universities, China University of Geosciences (Wuhan) (No. CUGL180402).

-
- [1] J. S. Schwinger, Phys. Rev. 82 (1951) 664.
 - [2] I. K. Affleck and N. S. Manton, Nucl. Phys. B 194 (1982) 38.
 - [3] J. M. Maldacena, Adv. Theor. Math. Phys. 2, 231 (1998).
 - [4] S. S. Gubser, I. R. Klebanov and A. M. Polyakov, Phys. Lett. B 428, 105 (1998).
 - [5] O. Aharony, S. S. Gubser, J. Maldacena, H. Ooguri and Y. Oz, Phys. Rept. 323, 183 (2000).
 - [6] G. W. Semenoff and K. Zarembo, Phys. Rev. Lett. 107 (2011) 171601.
 - [7] Y. Sato and K. Yoshida, JHEP 04 (2013) 111.
 - [8] Y. Sato and K. Yoshida, JHEP 08 (2013) 002.
 - [9] Y. Sato and K. Yoshida, JHEP 09 (2013) 134.
 - [10] Y. Sato and K. Yoshida, JHEP 12 (2013) 051.
 - [11] S. Chakraborty and B. Sathiapalan, Nucl. Phys. B 890 (2014) 241.
 - [12] K. B. Fadafan and F. Saiedi, Eur. Phys. J. C (2015) 75:612.
 - [13] M. Ghodrati, Phys. Rev. D 92, 065015 (2015).
 - [14] L. Zhang, D. f. Hou and J. Li, Eur. Phys. J. A (2018) 54:94.

- [15] Z.-q. Zhang, X. R. Zhu and D. f. Hou, Phys. Rev. D 101, 026017 (2020).
- [16] Z.-q. Zhang, Nucl. Phys. B 935 (2018) 377.
- [17] L. Shahkarami, M. Dehghani, P. Dehghani, Phys. Rev. D 97, 046013 (2018).
- [18] W. Fischler, P. H. Nguyen, J. F. Pedraza, W. Tangarife, Phys. Rev. D 91, 086015 (2015).
- [19] Z. R. Zhu, D. f. Hou, Xun Chen, Eur. Phys. J. C (2020) 80:550.
- [20] K. Hashimoto and T. Oka, JHEP 10 (2013) 116.
- [21] K. Hashimoto, T. Oka, and A. Sonoda, JHEP 06 (2014) 085.
- [22] X. Wu, JHEP 09 (2015) 044.
- [23] K. Ghoroku, M. Ishihara, JHEP 09 (2016) 011.
- [24] D. Kawai, Y. Sato, K. Yoshida, Internat. J. Modern Phys. A 30 (2015) 1530026.
- [25] J. Erlich, E. Katz, D. T. Son and M. A. Stephanov, Phys. Rev. Lett. 95, 261602 (2005).
- [26] J. Polchinski, M. J. Strassler, JHEP 05 (2003) 012.
- [27] A. Karch, E. Katz, D. T. Son and M. A. Stephanov, Phys. Rev. D 74, 015005 (2006).
- [28] J. P. Shock, F. Wu, Y-L. Wu and Z-F. Xie, JHEP 03 (2007) 064.
- [29] A. Stoffers and I. Zahed, Phys. Rev. D 83, (2011) 055016.
- [30] D. n. Li and M. Huang, JHEP 11 (2013) 088.
- [31] D. n. Li, S. He, M. Huang and Q. S. Yan, JHEP 09 (2011) 041.
- [32] S. He, M. Huang and Q. S. Yan, JHEP, Phys. Rev. D 83, 045034 (2011).
- [33] S. He, S. Y. Wu, Y. Yang and P. H. Yuan, JHEP 04 (2013) 093.
- [34] R. Rougemont, A. Ficnar, S. Finazzo and J. Noronha, JHEP 04 (2016) 102.
- [35] P. Colangelo, F. Giannuzzi and S. Nicotri, Phys. Rev. D 83, (2011) 035015.
- [36] C. Park, D.-Y. Gwak, B.-H. Lee, Y. Ko and S. Shin, Phys. Rev. D 84, (2011) 046007.
- [37] P. Colangelo, F. Giannuzzi and S. Nicotri, JHEP 05 (2012) 076.
- [38] P. Colangelo, F. Giannuzzi, S. Nicotri and F. Zuo, Phys. Rev. D 88 (2013) 115011.
- [39] Y. Xiong, X. Tang, and Z. Luo, Chin. Phys. C 43, 113103 (2019).
- [40] X. Chen, S.-Q. Feng, Y.-F. Shi, Y. Zhong, Phys. Rev. D 97, 066015 (2018).
- [41] Z.-q. Zhang and X. R. Zhu, Phys. Lett. B 793 (2019) 200.
- [42] O. Andreev and V. I. Zakharov, Phys. Rev. D 74, 025023 (2006).
- [43] M. Cvetič, et al., Nucl. Phys. B 558 (1999) 96.
- [44] D. T. Son and A. O. Starinets, JHEP 03 (2006) 052.
- [45] H. Liu, K. Rajagopal and Y. Shi, JHEP 08 (2008) 048.